BULMAN RESOURCES PTY LTD

FIXED WING AIRBORNE SURVEY OF BULMAN PROJECT, NORTHERN TERRITORY

Project Number 2256

TECHNICAL REPORT ON GEOLOGICAL INTERPRETATION OF AIRBORNE MAGNETIC AND ELECTROMAGNETIC DATA

Survey conducted by

Fugro Airborne Surveys Pty Ltd
435 Scarborough Beach Road,
Osborne Park
Western Australia, 6017
AUSTRALIA
Tel: +61 (0) 8 9273 6400 Fax: +61 (0) 8 9273 6466
Email: interpretation@fugroairborne.com.au

Contributing authors:	Dr. Peter Kovac, Dr. Jacqueline Hope
Internal QC:	Dr Jurriaan Feijth
Authorised for release by:	Dr. Simon Wetherley; Interpretation Manager
Version number:	1.0
Date:	21st December 2011

ABSTRACT

This report documents the interpretation of the airborne TEMPEST electromagnetic (EM) and magnetic data acquired in August, 2011 by Fugro Airborne Surveys Pty. Ltd. (FAS) for Bulman Resources Pty. Ltd. over the Bulman project area. The primary aim of the integrated interpretation was to determine the 3D geometry of the dolerite sills in the area and to identify any discrete bedrock conductors using the recently acquired EM and magnetic data.

Interpretation of magnetic data shows dolerite sills and dykes in the eastern, southern and western parts of the Bulman Prospect, respectively. The difference in their magnetic response is interpreted as a function of the depth and timing of their emplacement. The location of the sills and dykes within the Bulman Prospect area was mapped using magnetic while depth estimations were derived from the EM data. To calculate the top of the intrusives, depth to resistive basement was mapped using Conductivity Depth Images (CDIs) generated from the TEMPEST B-field Z component data. Additionally, a voxel model was constructed from the CDIs to show the conductivity distribution beneath the survey area in three dimensions. The overall conductivity pattern of the Bulman Project indicates that dolomitic sandstone and siltstone of the Dook Creek Formation are more conductive than overlying coarse sandstone of the Limmen Formation. A disconformable boundary between the Dook Creek Formation and the Limmen Formation shows as a distinct interface in the EM data. There is no marked conductivity contrast between the Derim-Derim intrusives and other rocks making up the resistive basement. As a result, the picked depth to resistive basement horizon corresponds to (a) the bottom of a surface conductive unit interpreted to be the base of the Cenozoic unconsolidated deposits, (b) a part of the Dook Creek Formation, and (c) in places, the base of a sub-surface conductive zone interpreted to be the top of the Derim-Derim intrusives. The thickness of sediments above the resistive basement is variable, reaching up to 170 metres in the central - eastern part of the tenement

To identify discrete bedrock conductors, electromagnetic anomaly picking was carried out using both the X- and Z-components of the B-field response, and discrete anomalies were subsequently ranked. The EM anomaly picks have been sorted into nine ranking categories, based on both their EM and magnetic response. In the ranking scheme employed for this report, a rank of A-1 denotes anomalies with the greatest potential for mineralisation, while C-3 represents anomalies with the least potential.

CONTENTS

FIGURES

TABLES

1 INTRODUCTION

This report documents the interpretation of the airborne TEMPEST electromagnetic and magnetic data acquired in August, 2011 by Fugro Airborne Surveys Pty. Ltd. (FAS) for Bulman Resources Pty Ltd over the Bulman project area.

The deposit style at the Bulman Project appears to fall within the stratabound carbonate-hosted class. Pb-Zn mineral occurrences are hosted by carbonates of the Dook Creek Formation. Known Pb-Zn occurrences in the south of the area of interest (EL 23814) have been interpreted as being underlain by a sill of Derim Derim Dolerite that has intruded the host unit, the Dook Creek Formation (Admirality Resources NL, 2008). This correlates with the limited historical drill data. The two best mineralised areas lie along two major NW-trending structures. An apparent NE trend of mineralised “lodes” at these prospects indicates a likely NE structural trend locating the deposit (Admirality Resources NL, 2007).

The primary aim of the integrated interpretation was to determine the 3D geometry of the dolerite sills in the area and to identify any discrete bedrock conductors.

The following data have been used for the interpretation project:

- Newly acquired TEMPEST EM data
- Newly acquired magnetic data
- Published geological data

Technical details of the TEMPEST airborne electromagnetic survey:

Electromagnetic Data Sample rate	0.2 seconds
Magnetic Data Sample Rate	0.2 seconds
Nominal Terrain Clearance	100 metres
Flight Line Spacing	200 metres
Tie Line Spacing	2000 metres
Flight Line Trend	90 degrees
Tie Line Trend	0 degrees
Line kilometres	1397 kilometres

2 GEOLOGICAL SUMMARY

The Bulman Project is a lead and zinc oxide deposit located in southern Arnhem Land in Australia's Northern Territory. The regional geological structure consists of Proterozoic McArthur Basin rocks including the Katherine River Group, Mt Rigg Group and Roper Group. The principal tectonic feature is the northwest trending Bulman Fault.

2.1 Lithology

The Bulman project area consists of Proterozoic sedimentary sequences of the McArthur Basin, including the Dook Creek Formation, which is overlain by the Limmen Formation. Both formations are thought to be intruded by dolerite sills and dykes. The prospect is largely covered by unconsolidated deposits ranging in age from the Cainozoic to the Quaternary.

Quaternary unconsolidated cover consists of gravel, sand, silt and clay. The rocks represent channel and floodplain deposits, as well as minor ephemeral lake deposits. Cainozoic unconsolidated material is composed of gravel, sand, silts and minor limestone in the form of undivided residual soil, colluvium, older alluvium and spring deposits. The Cainozoic to Quaternary deposits in the McArthur Basin underwent widespread deep-weathering and silicification events in the Cretaceous and in the Cainozoic (Sweet and Brakel, 1999).

The Mesoproterozoic Limmen Sandstone is quartz rich to sublithic, fine- to coarse-grained silicified sandstone, which lies disconformably over the Dook Creek Formation (Sweet and Brakel, 1999). The Limmen Sandstone is a part of the Roper Group of sediments.

The underlying Mesoproterozoic Dook Creek Formation is composed of dololutite, dolomitic sandstone and siltstone, stromatolitic and oolitic dolostone, chert, quartz sandstone, conglomerate, mudstone, siltstone. It is a part of the Mount Rigg Group of sediments. The Dook Creek Formation is intensely weathered and silicified to a depth of 20 metres. The outcrop and sub-crop belt of the Dook Creek Formation is paralleled by a belt of sinkholes, developed in the carbonates as a consequence of deep weathering and its accompanying effects (Sweet and Brakel, 1999). The Dook Creek Formation is believed to be a major aquifer in the area of interest (Knapton, 2009). The aquifers of the Dook Creek Dolostone are typical of karstic aquifers where chemical weathering has produced widespread secondary porosity and permeability in the

carbonates. The carbonate aquifers are expected to have greatest permeability within the weathered zone, up to a maximum of 100 – 150 metres below the surface (Knapton, 2009).

Fine- to coarse-grained dolerite and gabbro sills and dykes, referred to as Derim Derim Dolerite (Sweet and Brakel, 1999), intrude, and are emplaced within, the Mount Rigg and Roper Groups.

2.2 Tectonics

Faults systems and regional lineaments from existing geological maps (Roberts et al., 1963; Sweet and Brakel, 1999; Rawlings, 2001) and studies (Admirality Resources NL, 2007; Admirality Resources NL, 2008) show regular northwest, north, and northeast trends. The principal tectonic structure of the Bulman Prospect area is the Bulman Fault. The fault system is a dominant northwest-trending regional structure running across the north-western part of the McArthur Basin (Rawlings, 2001).

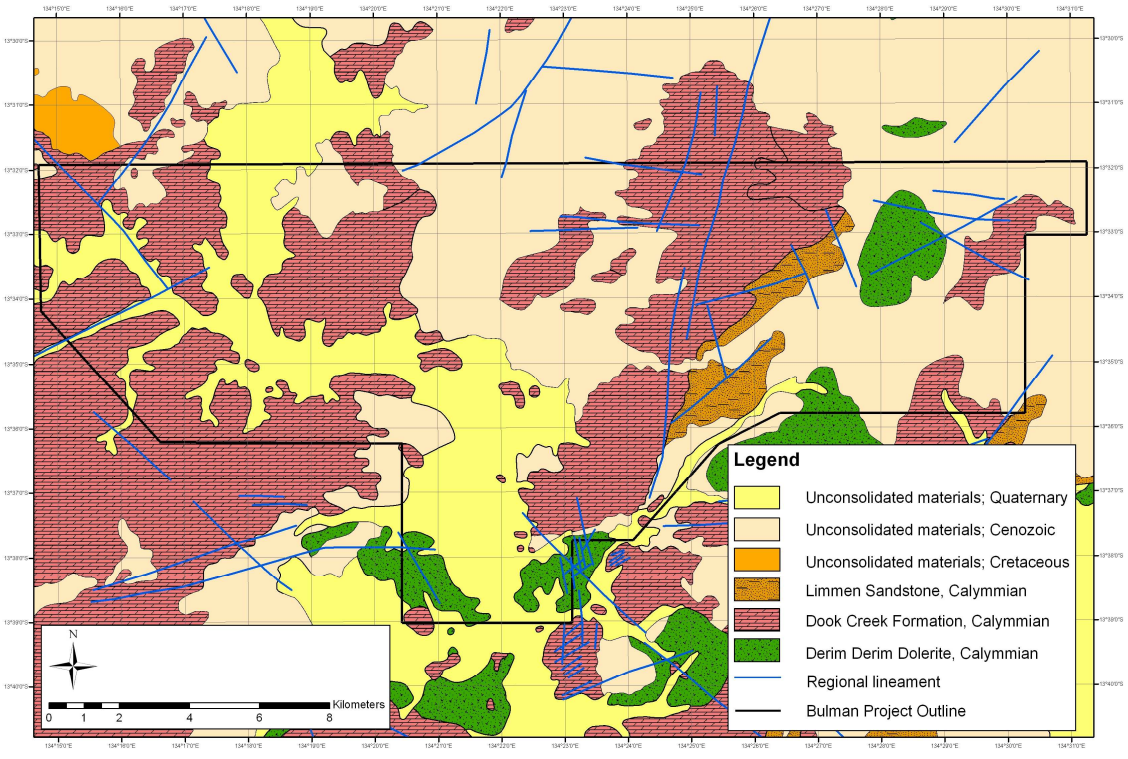

Figure 2.1 Geological map of the Bulman Project area, Northern Territory (after Sweet and Brakel, 1999)

3 INTERPRETATION OF ELECTROMAGNETIC DATA

The aim of the EM depth to resistive basement interpretation was to identify the top of the sills in the project area. To accomplish this, depth to resistive basement was mapped using Conductivity Depth Images (CDIs) generated from the TEMPEST B-field Z component data. Additionally, a voxel model was constructed from the CDIs to show the conductivity distribution beneath the survey area in three dimensions. Electromagnetic anomaly picking was carried out using both the X- and Z-components of the B-field response and discrete conductors were subsequently ranked.

3.1 Depth to Resistive Basement

CDIs generated from the TEMPEST B-field Z component data were used to map identifiable conductivity contrasts within the geological units. CDIs were produced using EM Flow software (Macnae et al., 1991; Macnae et al., 1998) and are an effective transformation of AEM data provided the input data is well calibrated, broadband and low noise.

Care must be taken when interpreting CDIs for a number of reasons, many related to the uncertainty of the value of 1-D model fitting in 2-D and 3-D situations:

- CDIs are relatively fast to compute, but have a tendency to overestimate shallow conductivities (Hunter and Macnae, 2001), are more sensitive to noise, and don't allow quantitative model assessment as a full model misfit error is not derived

- Rugged topography represents some of the biggest limitations as: (1) the surface is not flat as modelled; (2) the transmitter-receiver geometry deviates from its nominal geometry; and (3) aircraft manoeuvres cause coil motion-induced noise

- Due to the methodology used to generate CDIs (a simple layered earth model is assumed), it is not possible to accurately represent discrete conductors (Figure 3.1).

- Edge effects are observed with AEM data at vertical contacts, which introduces artefacts in models fit with a 1-D assumption. These edge effects are emphasised by the slight asymmetrical system configuration of the TEMPEST system. Lagging has been applied for horizontal features.

- Late-time decays are modelled with a power-law assumption, whereas 3-D conductors have exponential decays at late times. Nevertheless, Ellis (1995) has shown that for the AEM system geometry, 1-D models usually give reasonable results when compared to full 3-D computations

- Ignoring current channelling effects, a 1-D assumption models only the earth's inductive response. Also disregarded are effects from magnetic permeability and induced polarisation (IP). Modelling results have shown that EM responses due to the magnetic permeability of the subsurface can be ignored for fixed-wing surveys (Sattel, 2000) and IP effects are only observed in very resistive environments (Smith and Klein, 1996).

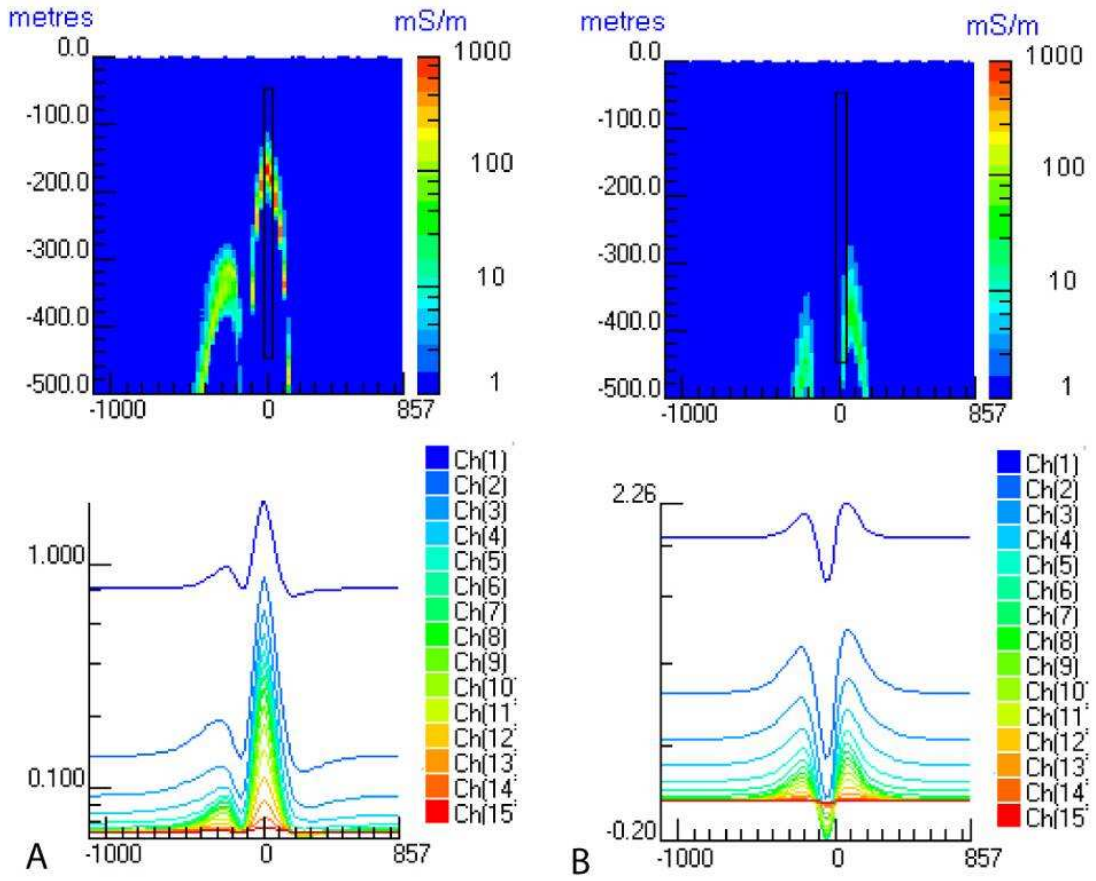

Figure 3.1: CDI sections and response profiles for a vertical plate model in a resistive background, simulating a bedrock conductor. (A) X-component and (B) Z-component. Model response calculated using program "LeroiAir". A 100S vertical plate of dimensions 400m by 400m, shown as a black rectangular outline, was placed at a depth of 50m in a 1mS/m host.

CDIs are usually displayed using a vertical exaggeration. This representation can make dipping contacts appear as vertical or sub-vertical contacts. This effect must be taken into consideration when interpreting CDI sections. CDIs are particularly useful in areas where a 1-D assumption within the 'footprint' of the system is a reasonable

approximation (e.g. areas with extensive conductive regolith or with flat-lying or shallow dipping lithologies). The Z-component of the electromagnetic field was utilised for the generation of CDIs as this component is the most sensitive to sub-horizontal layered earth environments.

The aim of the EM depth to resistive basement interpretation was to map the interface between conductive cover and resistive 'basement'. Ideally, this should map the contact between conductive sediments and the underlying resistive basement, including the Derim-Derim intrusive sills. In this area, there are two main complications:

(1) When a conductive layer is present at or near surface, it may mask everything below it depending on the thickness and conductivity of the layer.

(2) Unfortunately, in this area, there is no marked conductivity contrast between the Derim-Derim intrusives and other rocks making up the resistive basement.

As a result, the resistivity contrast boundary that was picked (Figure 3.2) corresponds both to the bottom of a surface conductive unit interpreted to be the base of the Cenozoic unconsolidated deposits and a part of the Dook Creek Formation, and, in places, the base of a sub-surface conductive zone interpreted to be the top of the Derim-Derim intrusives.

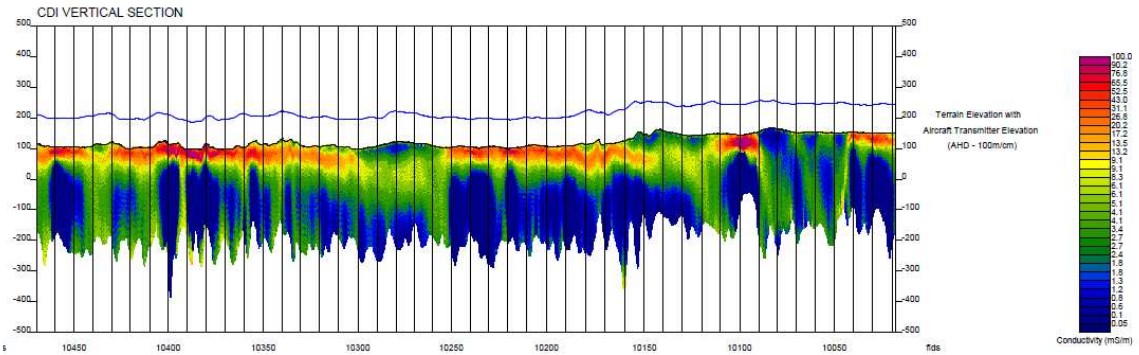

Figure 3.2: Example of CDI image for Line 1001702 showing the surficial conductive zone (red) corresponding the Cenozoic unconsolidated deposits and part of the Dook Creek Formation

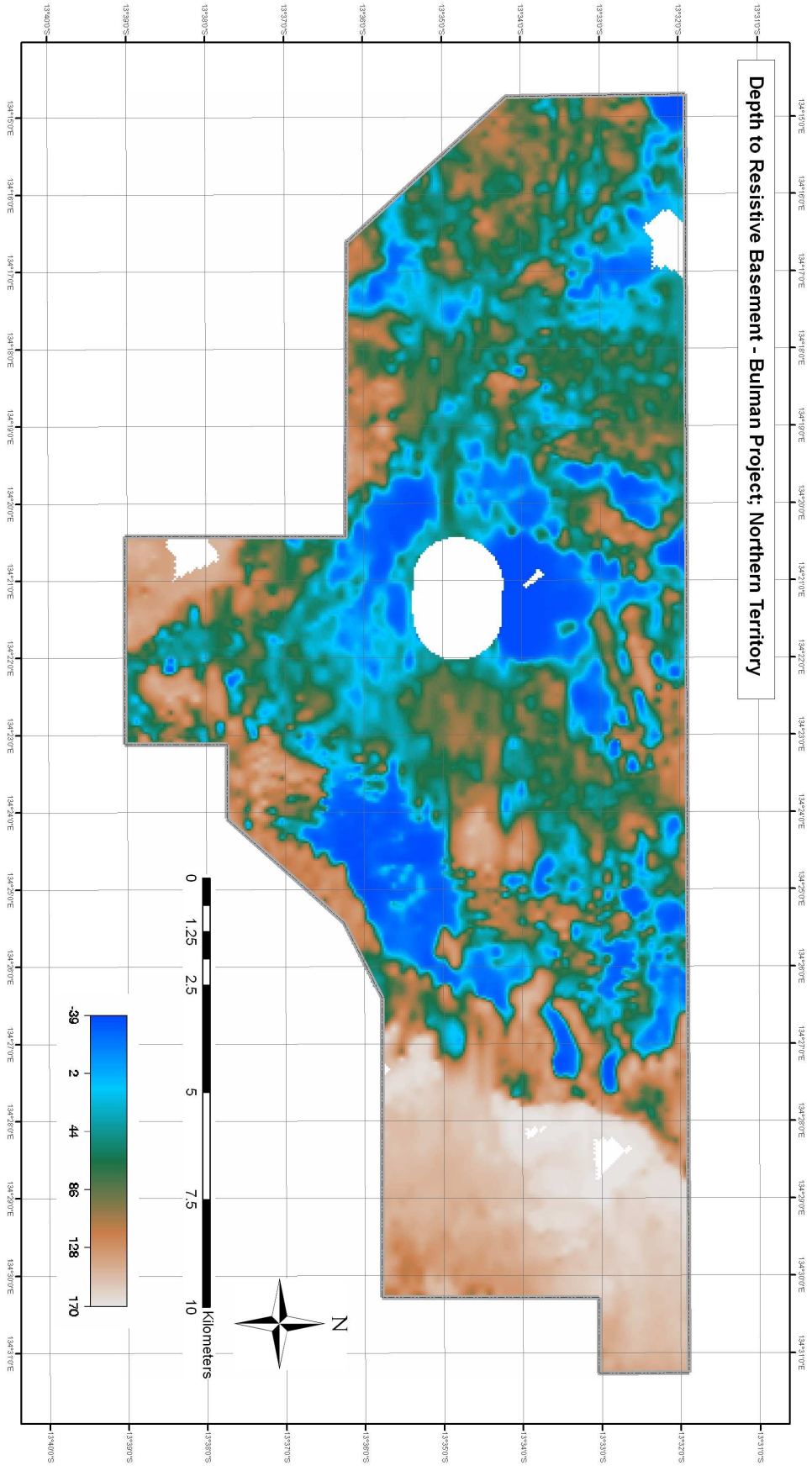

Figure 3.3: Depth to resistive basement map for the Bulman Project area

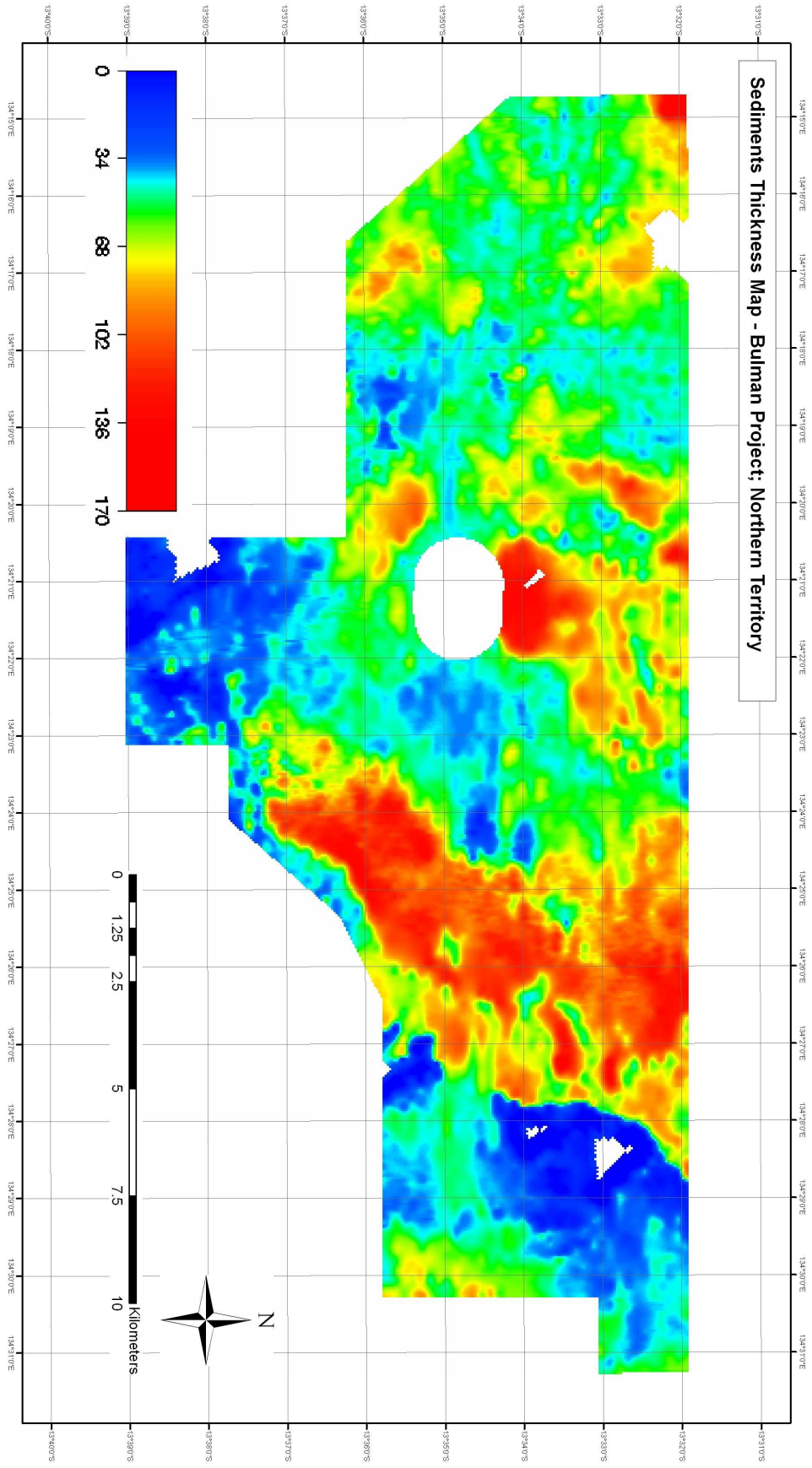

Figure 3.4 Sediment thickness map for the Bulman Project area

Figure 3.3 is a grid of the digitized horizon representing the base of the Cenozoic unconsolidated deposits and a part of the Dook Creek Formation. When this surface is subtracted from the digital elevation model (DEM), the thickness of the conductive layer (Figure 3.4) has been calculated. For the Bulman Project study area the thickness of sediments above the resistive basement is variable, reaching up to 170 metres in the central - eastern part of the tenement.

3.2 Conductivity Distribution in Three Dimensions

Using the CDI data, it is possible to generate 3-D voxel models representing the conductivity distribution beneath the survey area in three dimensions. Visualisation and analysis of the data can then be undertaken to assist with the geological interpretation and to identify electromagnetic anomalies of interest. For the purposes of this project, Pitney Bowes' (Encom) PA software was used for visualisation and analysis.

The 3-D voxel model is generated by:

i. Transforming depth values in the CDI array database to elevation using the DTM values

ii. Generating new array channels of Elevation and Interpolated Conductivity in the CDI database at increments of 5 m

iii. Calculating the three dimensional conductivity voxel model using the minimum curvature method

iv. Clipping the resultant voxel model by the DTM surface to remove anomalous above ground features that may result from the gridding.

From the 3-D voxel model a number of different visualisation techniques are possible. These include:

- Vertical and horizontal slices along planar surfaces
- Threshold volume displaying only voxels with conductivity values between a defined range
- Isosurfaces -- the 3-D extension of a 2-D contour line. This is a surface that joins together points with the same property value. In the case of this survey, that property is conductivity

Any interpretation drawn from the 3-D voxel model and the various imaging techniques should always be followed by a close inspection of the source CDIs. Although the 3-D visualisation allow for a much better understanding of the geology it will also contain all of the inherent problems of the CDI generation.

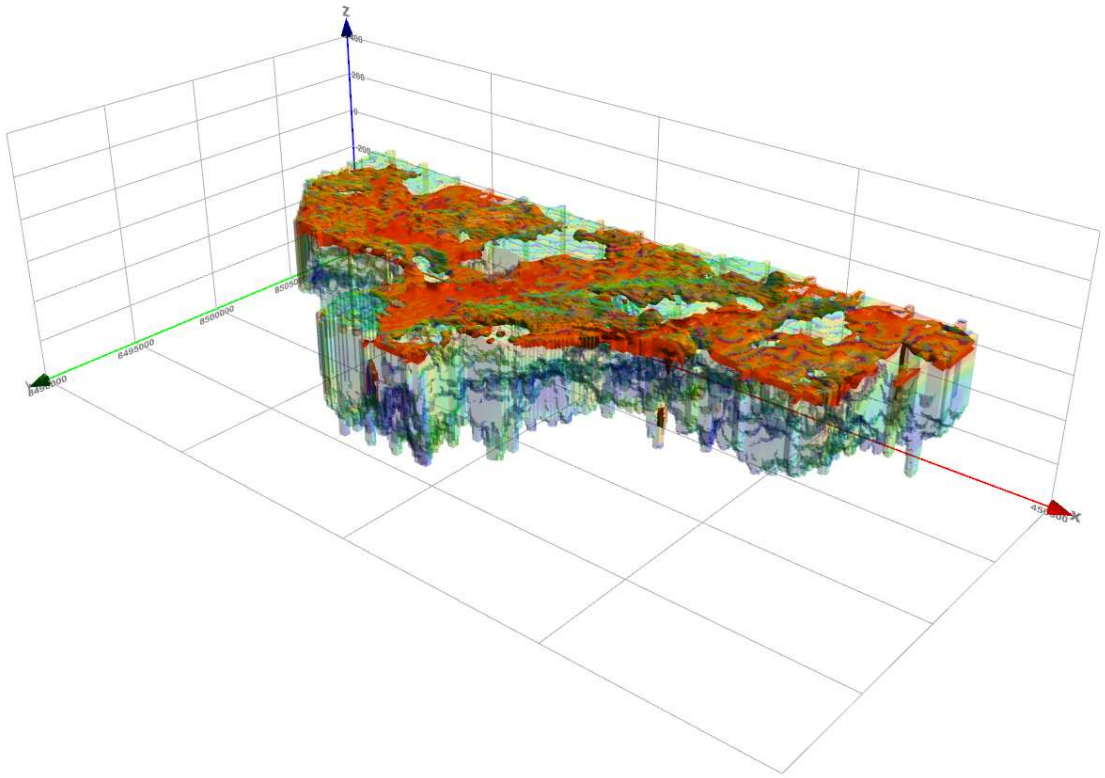

Figure 3.5: Semi-transparent 3-D voxel of EM data for Bulman Project with inserted 15mS/m isosurface corresponding to the bottom of a surface conductive unit interpreted to be the base of the Cenozoic unconsolidated deposits and a part of the Dook Creek Formation. View is from the southeast, looking northwest along the Bulman Fault.

A 3-D voxel model was generated for the entire Bulman Project, and is shown in Figure 3.5. In this figure, the voxel model is presented with a transparency applied, and an inserted 15 mS/m isosurface. This isosurface roughly corresponds to the bottom of a surface conductive unit interpreted to be the base of the Cenozoic unconsolidated deposits and a part of the Dook Creek Formation

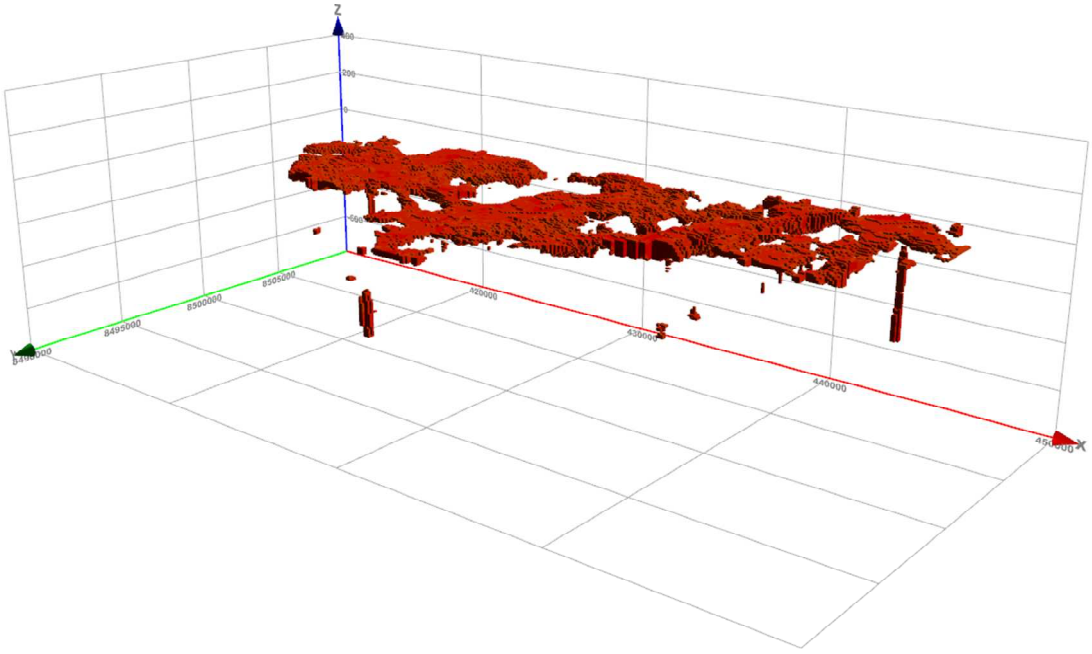

Figure 3.6: 3-D voxel for Bulman Project. Threshold volume displaying only voxels with conductivity values between 20mS/m and 110 mS/m.

3.3 Electromagnetic Anomaly Picking

Electromagnetic anomaly picking for the Bulman Project was done using both the X- and Z-components of the B-Field response. Although all components of the recorded EM data are viewed during anomaly picking, the X-component B-Field response is usually the best choice for identifying the positions of discrete bodies. Picking is generally done so that the point picked represents the position of the centre of the body responsible for the anomaly.

Only discrete anomalies can be picked. In areas of conductive overburden, or when many bodies are close enough that the EM anomalies merge or interfere with one another, discrete anomalies cannot be picked unless they clearly stand out from the background conductivity.

The following information is recorded in the CSV file provided to Bulman Resources:

Line	The line number that the anomaly pick falls on
Flight	The survey flight number
Bear	The bearing of the flight direction
Category	The anomaly type (see the table below)
ID	Anomaly identifier (upper case A, B, etc., lower case for culture)

FID	Fiducial at anomaly pick
X	X coordinate
Y	Y coordinate

Anomalies are identified by category based upon shape. The general categories are listed in Table 3.1.

EM anomalies generally follow conductive and resistive zones, which at many places represent boundaries of geological units and fault patterns. Some anomalies are randomly scattered within the studied block. Example images of typical anomaly picks are provided in Figure 3.7

CATEGORY IDENTIFIER	TYPE DESCRIPTION	ANOMALY DESCRIPTION
N	Normal (either plate-like or bedrock)	**Near vertical:** double, symmetric peak on Z & X crossover between Z peaks **Steeply dipping:** double, asymmetric peak on Z & X crossover between Z peaks **Shallowly dipping:** Single peak on Z & single peak on X shifted down-dip **Bedrock:** Indeterminate shape
C	Culture	Similar to N type, but with coincident powerline monitor response. Often these can have unusual decay characteristics. Cultural anomalies may occur without a powerline monitor response.
S	Surficial (flat-lying)	Single peak on both X and Z, coincident location
E	Edge	Edge between conductive and resistive zones

Table 3.1: EM anomaly category identifier, type, and anomaly description.

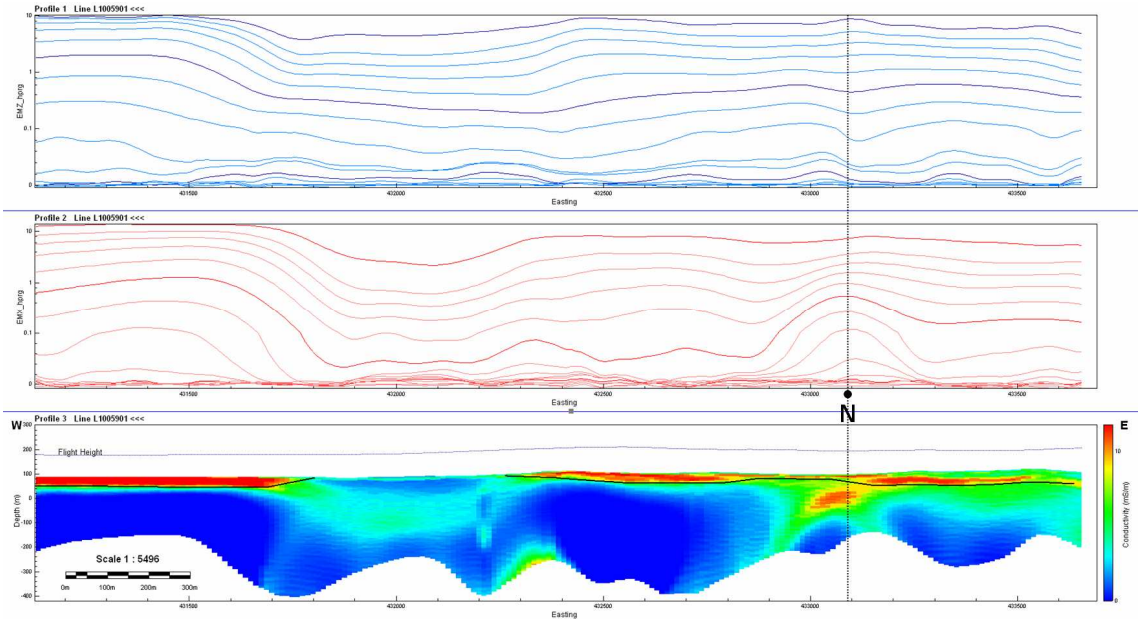

Figure 3.7: Shallowly dipping discrete bedrock conductor. Amplitudes for the anomaly are higher for later channels on both the B-Field Z (blue profile curves, top panel) and X (red curves, middle panel) components. The bottom panel shows the CDI for the line, which has been flown from east to west, with the depth to resistive basement pick (solid black line) overlaid.

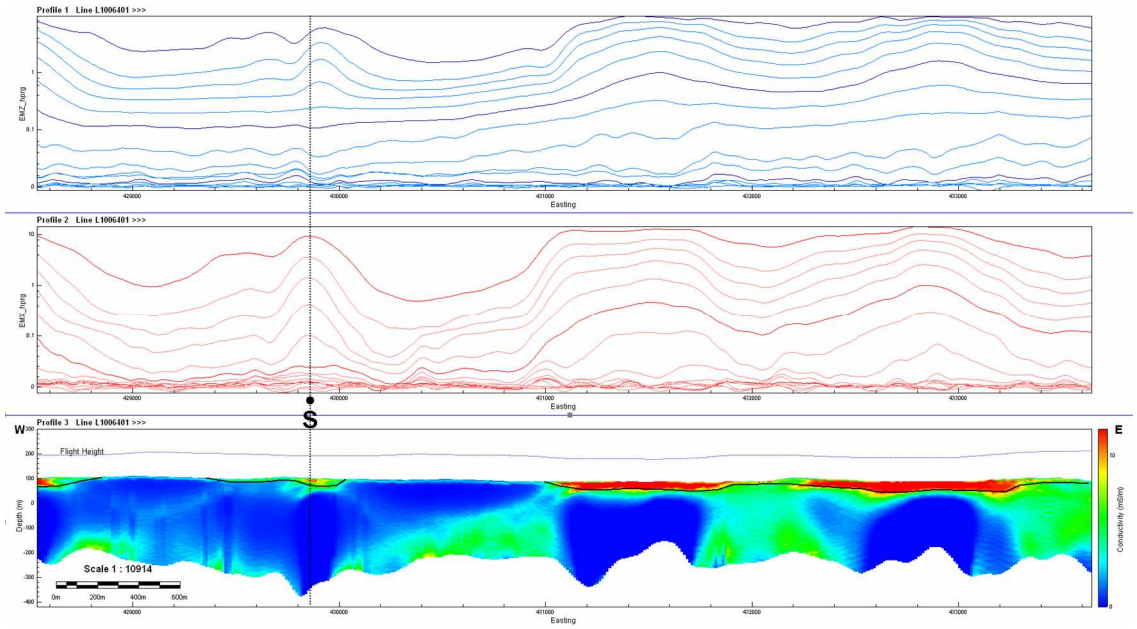

Figure 3.8: S-type (or Surficial) anomaly pick. Amplitudes of the near surface flat-lying conductor are largest for early channels, and drop off quickly after channel 5 for both the B-Field Z (blue curves, top panel) and X (red curves, middle panel) components. The bottom panel shows the corresponding CDI for the line, which has been flown from west to east, with the depth to resistive basement pick (solid black line) overlaid.

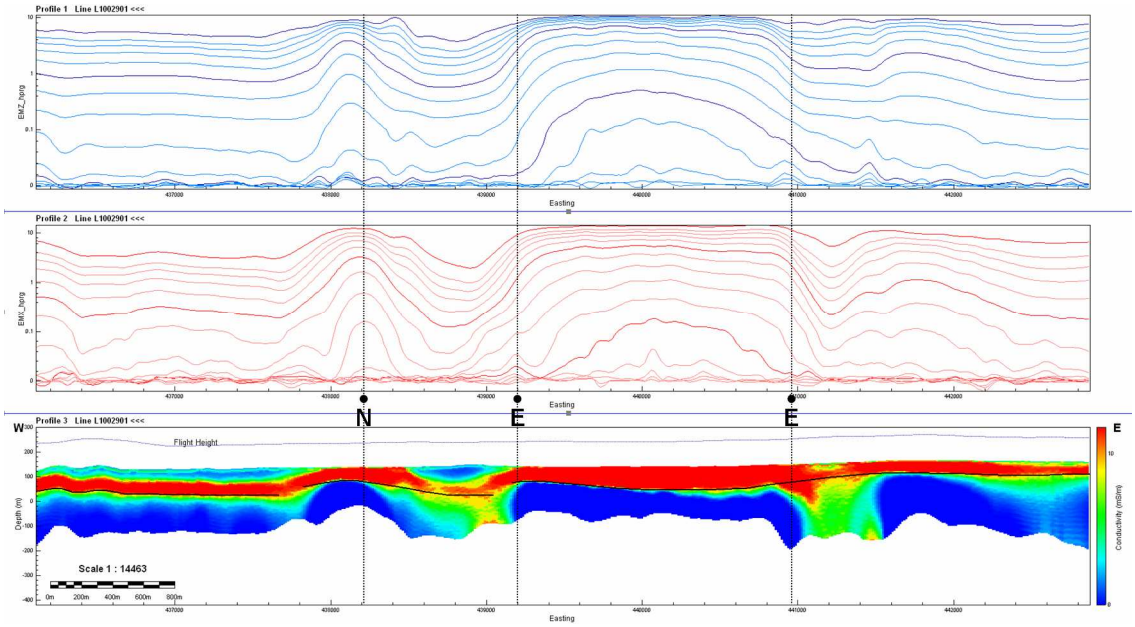

Figure 3.9: E-type anomaly pick, picking the edges of a change from thin, relatively resistive surface layer on the western end of the line to a strongly conductive near-surface unit in the middle of the profile. This unit is co-located with a river valley, observed on satellite data. On the mid-western end of the section shown here, a shallow N-type body has been picked. This body is masked in the conductive overburden, and likely represents a change in thickness and/or conductivity in the overburden. Amplitudes of the picked near-surface flat-lying conductor take longer to drop off than is observed in the case of typical S-type anomalies. The bottom panel shows the corresponding CDI for the line, which has been flown from west to east, with the depth to resistive basement pick (solid black line) overlaid.

3.4 Ranking of EM anomaly picks

The aim of anomaly picking is to identify anomalous responses. Electromagnetic anomaly picking is accomplished using both grids/maps and profiles. Some anomalies stand out in maps as somewhat isolated features along favourable structural intercepts; however, some localised changes in conductivity may only be apparent in profile form and not on maps because of the background conductivity. Generally, a review of EM anomalies is conducted on profiles to check for well-defined shapes, moderate amplitudes, and slow decay, and then checked against maps (EM, mag, etc) for strike length, structural support and overall conductivity pattern.

The EM anomaly picks are ranked using six criteria:

<u>Based on EM signature:</u>

A. Anomalous on maps and having good anomaly characteristics in profile form.

B. Non-distinct on maps, but having good anomaly characteristics in profile form.

C. Anomalous on maps, but lacking good characteristics in profile form.

Based on Magnetic signature:

1. With magnetic anomaly coincidence, suggesting a common source
2. Showing evidence of structural control from the magnetic data
3. Showing no support from the magnetic data

The EM anomaly picks are then sorted into nine categories, based on both their EM and magnetic response. The category assigned to each selection is shown in Table 3.2.

RANK	Response on maps	Profile expression	Magnetic signature
A-1	Anomalous	Good	Coincident anomaly
A-2	Anomalous	Good	Structural support
A-3	Anomalous	Good	No support
B-1	Non-distinct	Good	Coincident anomaly
B-2	Non-distinct	Good	Structural support
B-3	Non-distinct	Good	No support
C-1	Anomalous	Poor	Coincident anomaly
C-2	Anomalous	Poor	Structural support
C-3	Anomalous	Poor	No support

Table 3.2: EM anomaly rank identifier, and description of classification.

As some of the anomalies are quite extensive, often crossing many survey lines, ranking has been done on a selection of anomalies that represent the best type example (rather than classifying each anomaly on every line, which may at times become redundant). Conductors shown in plan view that are not assigned a ranking are generally bodies that display poor expression in both plan view and profile, and thus do not fit into any of the EM signature groups (A, B, or C). However, these conductors do display evidence of weakly conductive properties and are thus included in the conductor list.

In the ranking scheme employed for this report, a rank of A-1 denotes anomalies with the greatest potential for mineralisation, while C-3 represents anomalies with the least potential.

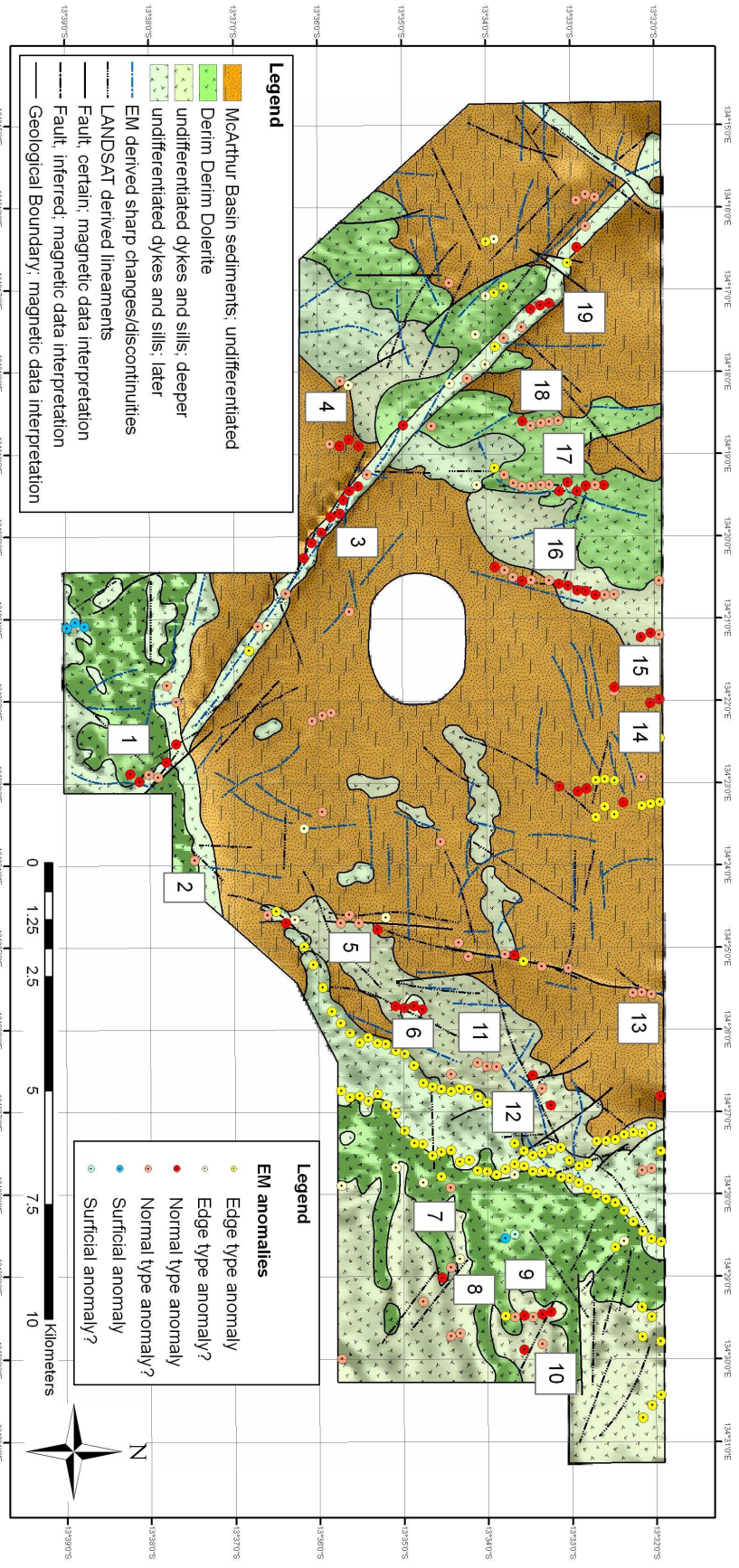

Figure 3.10 Map showing location of EM anomalies that have been ranked in Table 3.3, overlain on magnetic interpretation.

Cluster	Line Range	Best Response: Line/Anomaly ID	Observations	Rank
1	1005901-1005501	1005801/A	Anomaly shows on profiles as a shallow dipping to flat-lying conductor, and also shows well on B-Field X-component mid-channel maps. It is coincident with a magnetic anomaly associated with the Bulman Fault, and lies close to the Bulman Mine.	A-1
2	1005201	1005201/A	Anomaly shape is indeterminate, but has good amplitude for early channels on X- and Z-Component indicating shallow source - possibly surficial? Shows on early channel grids as part of an ENE-WSW striking linear feature, and is coincident with an ENE-WSW striking magnetic anomaly.	C-1
3	1004001-1003301	1003401/B 1003901/C 1004001/A	Anomaly shows on both X- and Z-component profiles for channels 1-7, and is visible in the early and mid channel grids. It is co-located with the Bulman Fault mag anomaly. Anomaly shape is indeterminate; possibly related to presence of intrusives along the fault giving rise to changes in thickness and/or conductivity of overburden?	C-1
4	1003401-1003701	1003401/A 1003501/E	Anomaly is visible on X- and Z-components for early to mid channels (1-6), and shows as a small amplitude N-S trending linear anomaly on B-Field X-component channel 6 grid, but does not have a coincident mag anomaly or structural support. Anomaly shape is indeterminate.	C-3
5	1003201-1003701	1003201/A	Expressed as a small amplitude anomaly with indeterminate shape on X- and Z-component early channel (1-5) profiles. Shows as a N-S trending edge to a broadly conductive zone in plan view, with a coincident shallow linear magnetic anomaly.	C-1
6	1002701-1003001	1002801/C 1002901/C	Shows as a single coincident peak on X- and Z-component profiles, suggesting shallow, flat-lying source. Anomaly is observed on channels 1-8, suggesting a fairly slow decay rate. In plan view, it shows as an isolated, high amplitude anomaly on both the X- and Z-component mid-channel grids, and is co-located with a magnetic anomaly suggestive of a common source. The anomaly is located close to the intersection of a NNW-SSE trending fault interpreted from the magnetic data and a NNE-SSW lineament observed on the Landsat data.	A-1
7	1002402	1002402/H	Anomaly expressed in profiles as shallowly-dipping conductor, with relatively quick decay (only visible on channels 1-5). In plan view, the anomaly shows on EM grids as a moderately low amplitude ENE-SSW trending high, The anomaly sits on the western end of a strong amplitude curvilinear magnetic anomaly.	A-2
8	1002302-1002701	1002502/A	Weakly conductive anomaly with an indeterminate shape on profiles, which is visible on channels 1-5. Anomalies plot along a NW-SE-trending high with moderate amplitude on the X- and Z-component grids. The NW-SE EM trend appears to be structurally supported by the magnetic data, with the anomalies plotting along a magnetic discontinuity.	C-2
9	1001301-1001801	1001601/H	Anomaly shows on profiles for channels 1-5, but has an indeterminate shape. In plan view, on the EM grids, the anomalies plot at the western edge of a broadly conductive zone, which coincides on the magnetic map with a discontinuity in the magnetic anomalies.	C-2
10	1001601	1001601/I	Moderately low amplitude anomaly with indeterminate shape on profiles, visible for early channels. In plan view, the anomaly shows as a moderate- to high-amplitude NW-SE trending linear anomaly in a broadly conductive zone, and is co-located with a magnetic discontinuity.	C-2
11	1001901-1002101	1001901/C	Anomaly is poorly expressed on profiles with weak amplitude and indeterminate shape, but can be seen on the X- and Z-component early channel grids. There is a coincident NNE-SSW trending positive magnetic anomaly with small amplitude on the magnetic maps.	C-1

Cluster	Line Range	Best Response: Line/Anomaly ID	Observations	Rank
12	1001301-1001501	1001301/D 1001501/D	Anomaly has indeterminate shape, and shows on profiles for early channels, but decays quickly. On the grids, the anomalies fall along a subtle EM high trending NE-SW, which is coincident with a positive magnetic anomaly. Anomalies lie along a NE-SW trending lineation interpreted on Landsat data, and close to the intersection with an interpreted NNW-SSE trending fault interpreted from the magnetic data.	C-1
13	1000201-1000401	1000201/E 1000301/G 1000401/B	Anomaly has an indeterminate shape on the X- and Z-component profiles, and is weakly conductive but decays fairly quickly (visible on channels 1-5). In plan view, the anomalies plot along a NNE-SSW linear high on both the EM and magnetic grids. Isolated anomalies have been picked along the same linear magnetic feature as it extends to the south, but the anomalies have poor expression in profile form, and do not show consistently from line to line.	C-1
14	1000101-1000201	1000101/I 1000201/B	Expressed as weakly conductive anomaly with moderately quick decay (visible on channels 1-6) and indeterminate shape on both X- and Z-component profiles. Anomaly shows as a moderate amplitude positive linear trend on both the X- and Z- component early channel grids, but there is no corresponding magnetic anomaly.	C-3
15	1000101-1000301	1000201/A	Anomaly shows as a weakly conductive, shallowly dipping conductor on X-and Z-component profiles that decays quickly (visible on channels 1-5). It shows as a moderate amplitude anomaly on early to mid channel EM grids. There is a strongly positive broad NE-SW trending linear magnetic anomaly just to the west of the EM anomalies that has been interpreted to be due to deeper volcanic intrusives.	A-2
16	1000602-1001301	1000802/C 1000902/D 1001002/D 1001102/D	Single peak on both X- and Z-component profiles indicates shallowly dipping to flat-lying source. Anomaly has high conductivity, a moderate decay rate, and is visible down to channel 8. This linear cluster of anomalies plots along a NE-SW trending broadly positive magnetic anomaly and has a coincident positive EM anomaly on both the X- and Z-component mid-channel grids.	A-1
17	1000701-1001701	1001102/E 1001202/B	Anomaly has moderate amplitude but indeterminate shape in profile form, and is expressed as a roughly N-S moderately high amplitude EM anomaly on the X- and Z-component mid-channel grids. The anomaly cluster lies along a linear N-S trending shallow magnetic anomaly.	C-1
18	1001201-1001601	1001601/B	Anomaly expressed as a moderate amplitude shallowly-dipping to flat-lying conductor on profiles, with peaks visible between channels 2-8. In plan view, the anomalies show as an N-S trending linear peak superimposed on a NE-SW-trending broadly conductive zone. On the magnetic data, the anomaly is co-located with a short wavelength (shallow source) magnetic high that, to the south, intersects with the broader and higher amplitude Bulman Fault magnetic anomaly.	A-1
19	1001301-1001501	1001301/H 1001401/A	Anomaly shows on profiles with moderate amplitude and indeterminate shape, and is visible on channels 1-8. In plan view, the anomalies fall on linear NNW –SSE trending moderate amplitude high on the X-component channel 6 grid, but the Z-component grid response is less readily apparent. The anomalies lie close to the magnetic anomaly associated with the Bulman fault, but are rotated slightly more towards the north.	C-2

Table 3.3 Ranked EM anomalies for Bulman survey area.

4 INTEGRATED GEOLOGICAL INTERPRETATION

The aim of the integrated geological interpretation of the Bulman Project was to understand the distribution of tectonic structures and lithological units. The integrated geological interpretation is based on the integration of geophysical data with other data such as previous mapping, tectonic sketches and various published papers. The process involved correlation with and extrapolation of information from geological units that outcrop to magnetic marker units or horizons and conductive layers (where available). All the data necessary to undertake the integrated interpretation were geo-rectified and placed within a geographic information system (GIS). Data capture (points, lines, and polygons) for all interpretation work was done on-screen and recorded directly in digital format and the data (points, lines, polygons) are fully attributed. The main interpretation files are the structural linework and the polygons created from this linework. The faults and polygons have been attributed according to magnetic response, EM response and interpreted geology.

The spatial distribution of rock magnetisation properties (or susceptibility and remanence) has been used for interpretation of the subsurface extent of geological units and structural elements with magnetic signal. The bulk susceptibility of rocks is controlled by the relative volume of ferromagnetic minerals that are present, especially magnetite. It is not uncommon to see reasonable variations in susceptibility within one single rock type. Hence, knowledge of susceptibility alone is not sufficient to determine rock type. Alternately, knowledge of rock type is often not sufficient to estimate expected susceptibility. Wide range in susceptibilities implies that spatial variations in the observed magnetic field may be readily related to geologic structure.

Electromagnetic (EM) data was used for delineation of the resistive basement surface and various conductive layers. An understanding of the regional geology for interpretation of EM data was vital, as is the response from the anticipated lithological interface. A related magnetic response was usually interpreted as signifying a lithological unit carrying the magnetic and conductive material.

The EM voxel model was used for visualisation in three dimensions. This voxel model was visualised as:

- Vertical and horizontal slices along planar surfaces

- Threshold volume displaying only voxels with conductivity values within a defined range

- Isosurfaces – a surface that joins together points with the same property value (in the case of this survey, conductivity)

The magnetic signal over the Bulman Project area results from the buried intrusives as the sediments of the McArthur Basin are magnetically 'transparent'. On the magnetic data, there are magnetically visible units in the eastern, southern and western parts of the Bulman Prospect (Figure 4.1). These have been interpreted in good accordance with previous survey results as possible dolerite sills of similar origin. Based on the intensity of their magnetic signal, three principal groups of intrusives have been distinguished. The difference in their magnetic response is interpreted as a function of the depth and timing of their emplacement. A high magnetic response appears to be related to outcropping or sub-surface intrusives, assigned in this report as the Derim Derim Dolerite in accordance with the existing geological maps (Roberts et al., 1963; Sweet and Brakel, 1999; Rawlings, 2001). Where the intrusives have been emplaced in lower levels of the McArthur basin sedimentary fill, magnetic responses with lower amplitude and frequency are observed. Both the dyke intruding along the north-west trending Bulman Fault and a north-east oriented dyke in the western part of the Bulman prospect show a high amplitude, short wavelength magnetic response. The trend of the dykes closely correlates with interpreted basement faults, suggesting these structures were used as pathways by the magma to intrude the McArthur Basin sedimentary sequence. Relative changes of the magnetisation vector between Derim Derim dolerite and dykes suggest a time sequence of magmatic events.

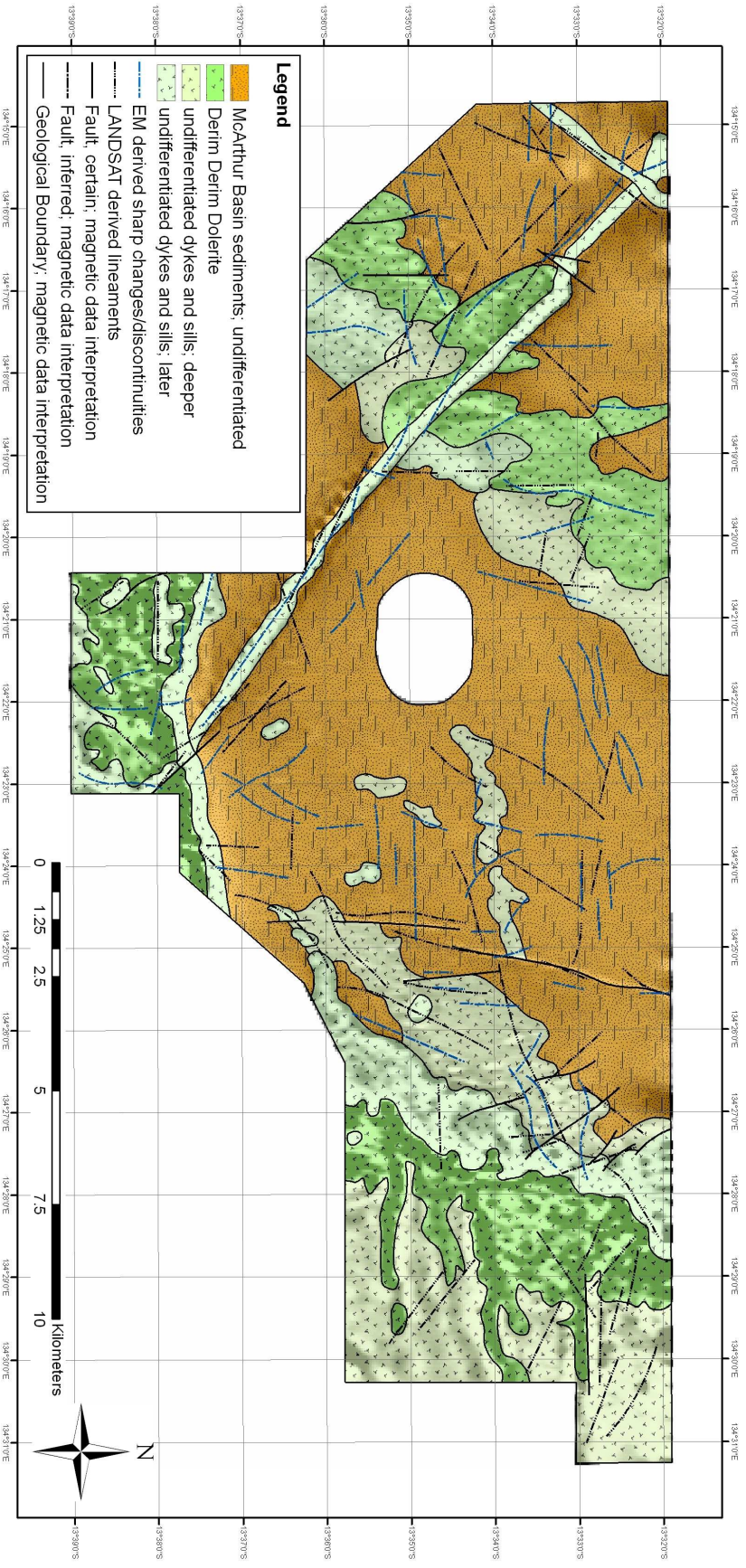

Figure 4.1 Interpretation of the Magnetic data overlain on First Vertical Derivate of Reduced to Pole Total Magnetic Intensity

The overall conductivity pattern of the Bulman Project is influenced by its lithological structure. Dololutite, dolomitic sandstone and siltstone of the Dook Creek Formation, which acts as a principal aquifer in the study area, appear to be more conductive than overlying coarse sandstone of the Limmen Formation. The conductivity signature of the formation is influenced by the lithological variability, its karstic character, the depth of weathering profile, and the level of the watertable. The disconformable boundary between the Dook Creek Formation and the overlying Limmen Formation is present in the electromagnetic data as a distinct conductivity interface. The Limmen Formation shows a fairly constant resistive electromagnetic response. It is indistinguishable from the Derim Derim Dolerite where the two are sharing a common boundary. It is only conductive when weathered. Intrusive bodies emplaced into the McArthur Basin sedimentary fill appear to be strong resistors, clearly imaged in the eastern part of the tenement where the Derim Derim dolerite crops out.

Conductivity characteristics for the sedimentary rocks and intrusives can be similar (Angenheister and G., 1982, Palacky; Figure 4.2), which makes it difficult to outline the boundary between the intrusives and sediments based on electromagnetic data only. Therefore, to better understand the emplacement of sills and dykes within the Bulman Prospect area, magnetic data has been used to define their location, and electromagnetic data has then been used to determine a minimum top intrusive depth (Figure 4.3).

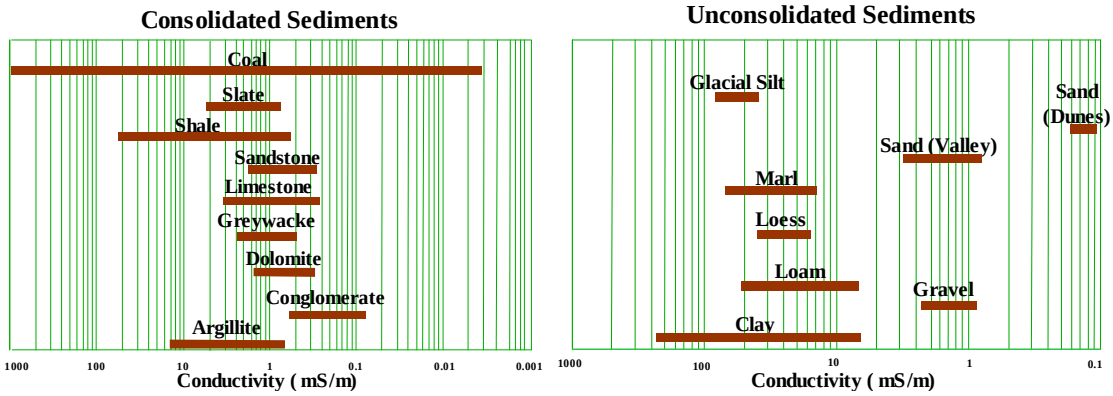

Figure 4.2 Conductivity range for different types of rocks (Angenheister and G., 1982)

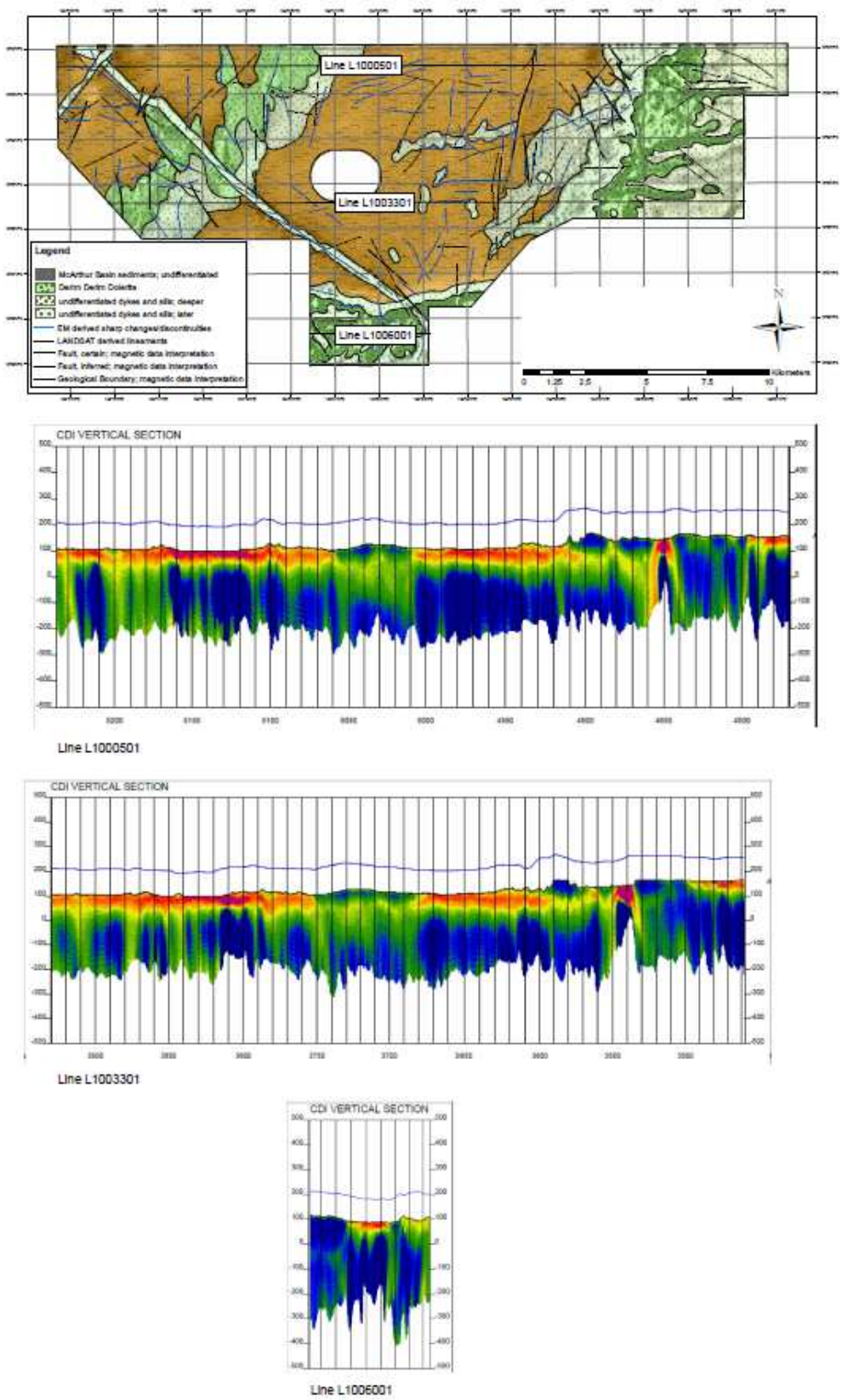

Figure 4.3 Interpretation of magnetic data showing subsurface location of the intrusive bodies and dykes (top). The locations of the CDI sections displayed below the map are shown with solid black lines. Magnetic data has been used to determine the extent of the sills and dykes, and their depth estimation is based on electromagnetic data

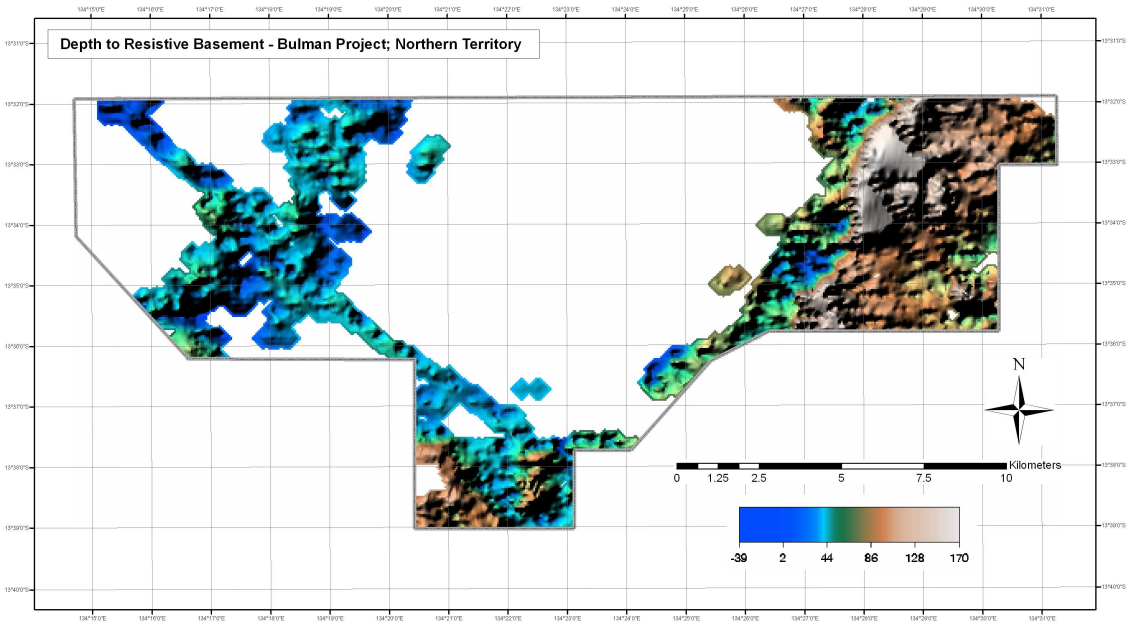

Figure 4.4 Depth to resistive basement surface, representing the shallowest possible Top of Intrusives horizon

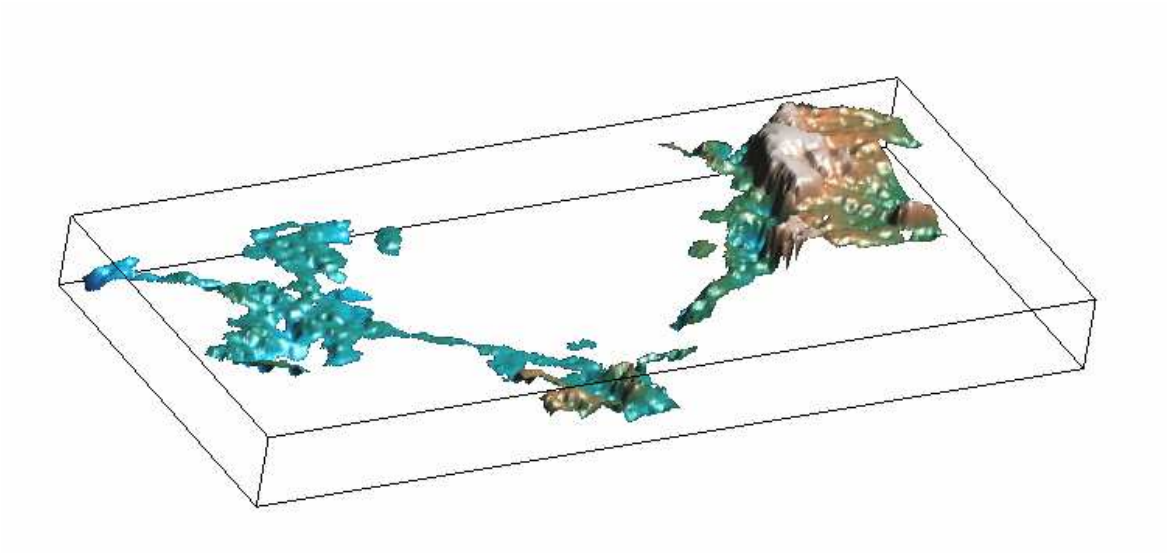

Figure 4.5 3D view of the topography of intrusive bodies, based on the depth to resistive basement interpretation

The surface conductivity layer appears to be largely influenced by the surface drainage pattern. The most conductive part of the surface conductive layer is located in the eastern part of the Bulman project, where it is interpreted to be related to unconsolidated alluvial sediments deposited in a north-south oriented valley. In the central and western part of the prospect area, the surface conductive layer is interpreted to be related to the Tertiary unconsolidated sediments and a weathered section of the Mesoproterozoic Dook Creek Formation.

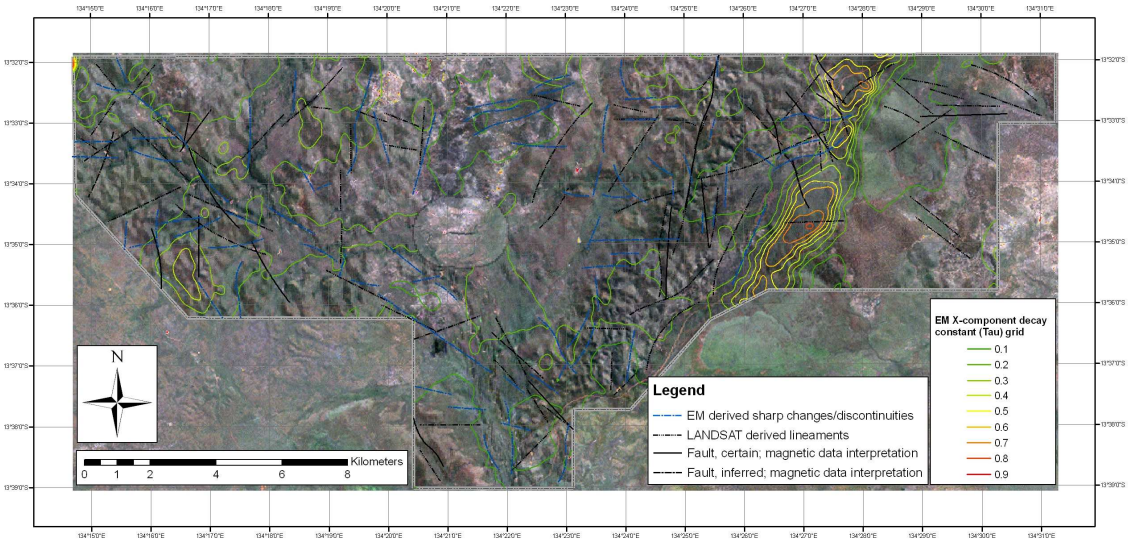

Figure 4.6 Landsat TM imagery overlain on DTM. Also shown are Tau contours, coloured according to decay rate. Areas with highest conductivities and slowest decay rates are co-located with recent unconsolidated drainage deposits in the eastern part of the prospect

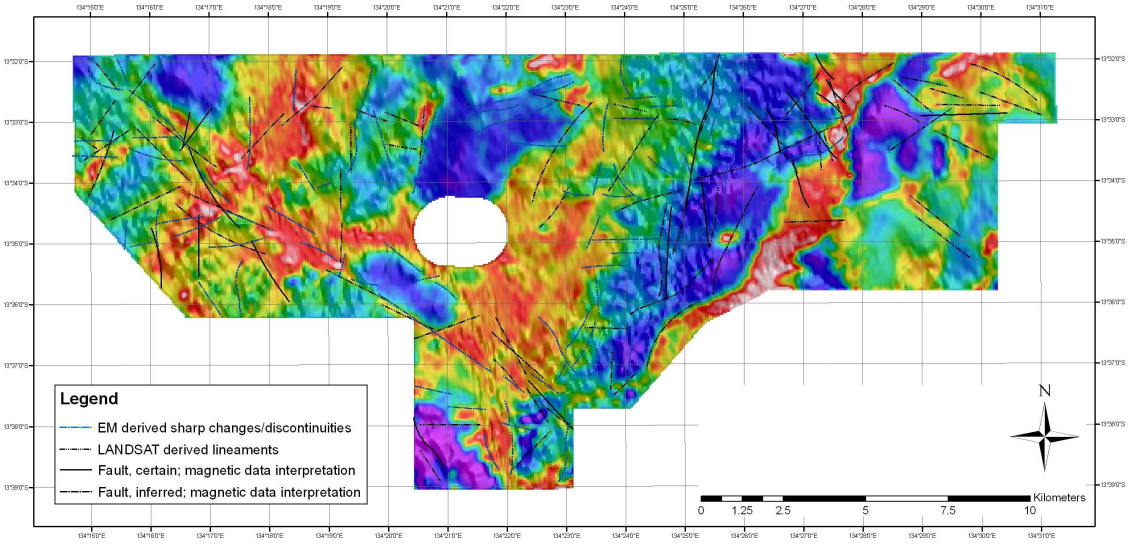

Figure 4.7 X-component Early Channels (average of channels 1-3) overlain on DTM; Surface conductive layer (in red) is interpreted to be related to Tertiary unconsolidated sediments and a part of the Mesoproterozoic Dook Creek Formation

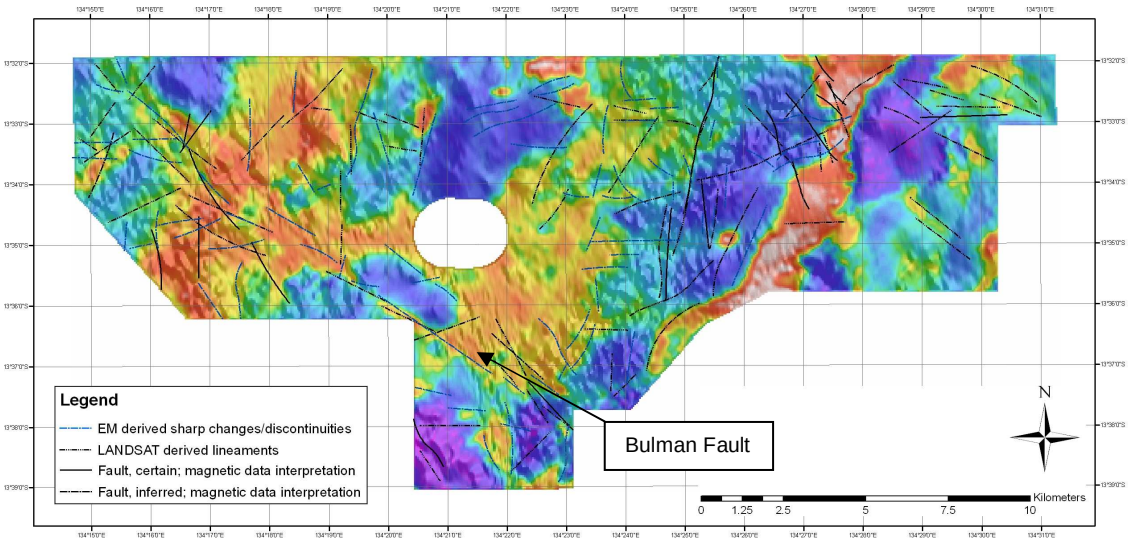

Figure 4.8 X-component Middle Channels (average of channels 5-7) overlain on DTM. The early and middle channels shows the surface conductivity layer related to the tectonic pattern, especially in the south-western part of the prospect where the Bulman Fault controls deposition of the Tertiary unconsolidated sediments.

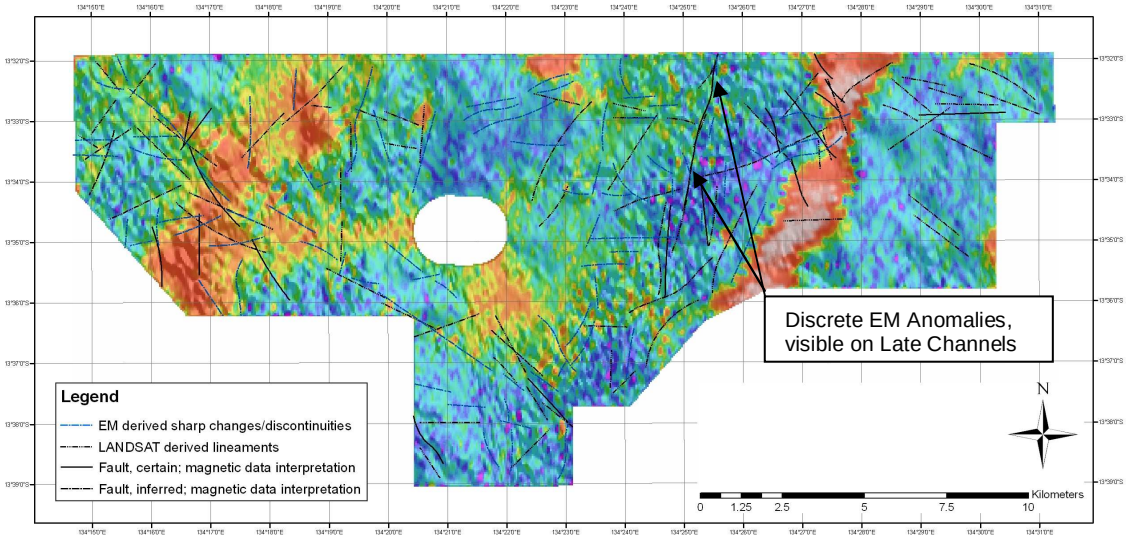

Figure 4.9 X-component Late Channels (average of channels 9-11) overlain on DTM. Discrete electromagnetic anomalies are notable in the eastern part of the project, possibly related to a north trending fault zone

The early and middle channels also suggest that near surface conductivities are influenced by regional tectonics, especially in the south-western part of the prospect where the Bulman Fault controls deposition of the Tertiary unconsolidated sediments.The geological interpretation of EM and magnetic data as well as Landsat TM imagery for the Bulman Project area is provided as ArcGIS digital files on the CD-ROM enclosed at the back of this report.

Shapefile	Description
Mag_Faults_LN	line shapefile; structural linework interpreted from magnetic data
EM_Anomalies	Points shapefile; EM anomalies picked from profile data
LANDSAT_Faults_LN	line shapefile; structural linework interpreted from Landsat imagery
Contour_TauX	line shapefile; EM X-component decay constant (Tau) grid derived contours
Contour_TauZ	line shapefile; EM Z-component decay constant (Tau) grid derived contours
EM_Discontinuities_LN	line shapefile; sharp changes/discontinuities derived from EM Ternary dataset and Depth to Resistive Basement
Bulman_Outline	line shapefile; Bulman Project outline
Bulman_LN	line shapefile; geological boundaries and tectonic structures interpreted from magnetic data
Bulman_PLY	polygon shapefile; polygons representing various lithologies interpreted from magnetic data
Bulman_PT	point file; points attributed form magnetic data according to interpreted geology

5 CONCLUSIONS

Several key issues have been recognised during this interpretation:

Some magnetic responses evident in the survey area appear to be result of interference from several magnetic sources. This may include magnetic responses of intrusive bodies from different geological depths that overlap each other.

Two principal EM layers have been recognized in the survey area. The conductive unit represents weathered unconsolidated Quaternary and Cainozoic sediments and a part of the Mesoproterozoic Dook Creek Formation. The base of this conductive layer is interpreted in places (with constraints provided by magnetic data) to be the top of intrusive bodies emplaced into the McArthur Basin sedimentary fill. The resistive layer is represented by the Limmen Formation and the intrusives.

Two major fault trends have been recognised in the survey area, including NE-SW and NW-SE fault systems. The most prominent fault is the NW-SE oriented Bulman Fault. The tectonic pattern has been distinguished using multiple magnetic and electromagnetic datasets.

Zones of structural disruption often appear as linear magnetic highs. These structures are interpreted to be pathways allowing magma to intrude the sedimentary sequence.

Lithological boundaries have been recognised between the intrusives and sediments in the survey area. They have been defined indirectly, based on magnetic response and conductivity characteristics.

To identify discrete conductors, electromagnetic anomaly picking was carried out using both the X- and Z-components of the B-field response, and these conductors were then ranked using both their EM and magnetic responses. In the nine-category ranking scheme employed in this report, a rank of A-1 denotes anomalies with the greatest potential for mineralization, while C-3 represents anomalies with the least potential.

6 REFERENCES

Admirality Resources NL, 2007, ASX Company Announcement, *Australian Stock Exchange Limited*,

Admirality Resources NL, 2008, ASX Company Announcement, *Australian Securities Exchange Limited*,

Angenheister, and G., 1982, Physical Properties of Rocks

Ellis, R. G., 1995, Airborne electromagnetic 3-D modeling and inversion, *Exploration Geophysics*, v. 26, p. 138-143

Hunter, D. and Macnae, J. C., 2001, Subsurface conductivity structure as approximated by conductivity-depth transforms, *ASEG Extended Abstracts*, Brisbane, QLD

Knapton, A., 2009, An integrated surface – groundwater model of the Roper River Catchment, Northern Territory. Part C - FEFLOW Groundwater Model , Department of Natural Resources, Environment, The Arts & Sport. Water Resources Branch, Technical Report No. 32/2009D. Northern Territory Government

Macnae, J. C., A. King, N. Stolz, A. Osmakoff, and A. Blaha, 1998, Fast AEM data processing and inversion, *Exploration Geophysics*, v. 29, p. 163-169

Macnae, J. C., R. Smith, B. D. Polzer, Y. Lamontagne, and P. S. Klinkert, 1991, Conductivity-Depth Imaging of Airborne Electromagnetic Step-Response Data, *Geophysics*, v. 56, no. 1, p. 102-114

Rawlings, D. J., 2001, Tectonostratigraphy of the McArthur Basin (1:1 000 000), *Northern Territory Geological Survey*,

Roberts, H. G., A. S. Mikolajczak, and G. Matveev, 1963, Mount Marumba, Northern Territory – 1:250 000 Geological Map Series. Explanatory Notes, SD 53-6, *Australian Geological Survey Organisation and Northern Territory Geological Survey (National Geoscience Mapping Accord)*,

Sattel, D., 2000, The effect of magnetic anomalies on transient electromagnetic data, *Exploration Geophysics*, v. 31, p. 140-149

Smith, R., and J. Klein, 1996, A special circumstance of airborne induced-polarization methods, *Geophysics*, v. 61, p. 66-73

Sweet, I. P., and A. T. Brakel, 1999, Mount Marumba, Northern Territory – 1:250 000 Geological Map Series. Explanatory Notes, SD 53-6 (second edition), *Australian Geological Survey Organisation and Northern Territory Geological Survey (National Geoscience Mapping Accord)*,